European Journal of Pharmaceutical Sciences 176 (2022) 106234

Contents lists available at ScienceDirect

European Journal of Pharmaceutical Sciences

journal homepage: www.elsevier.com/locate/ejps

Lipid nanoparticle formulations for optimal RNA-based topical delivery to murine airways

A Tam [a,d,e], J Kulkarni [a,b,c], K An [a,c], L Li [d], DR Dorscheid [e], GK Singhera [e,f], P Bernatchez [e,f,g], GSD Reid [d], KYT Chan [b,c], D Witzigmann [a,b,c], PR Cullis [a,b,c], DD Sin [e], CJ Lim [d,*]

[a] NanoVation Therapeutics Inc. Vancouver, British Columbia, Canada
[b] NanoMedicines Innovation Network, Vancouver, British Columbia, Canada
[c] University of British Columbia (UBC), Department of Biochemistry and Molecular Biology, Vancouver, British Columbia, Canada
[d] Michael Cuccione Childhood Cancer Research Program, BC Children's Hospital Research Institute, University of British Columbia Vancouver, British Columbia, Canada
[e] University of British Columbia (UBC) Center for Heart Lung Innovation, St. Paul's Hospital, Vancouver, British Columbia, Canada
[f] Department of Medicine (Division of Respirology), UBC, Vancouver, British Columbia, Canada
[g] Department of Anesthesiology, Pharmacology & Therapeutics, University of British Columbia, 217-2176 Health Sciences Mall, Vancouver, British Columbia V6T 1Z3, Canada

ARTICLE INFO

Keywords:
Lipid nanoparticles
mRNA
siRNA
Airway epithelial cells
Nasal cavity

ABSTRACT

Introduction: Lipid nanoparticles (LNP) have been successfully used as a platform technology for delivering nucleic acids to the liver. To broaden the application of LNPs in targeting non-hepatic tissues, we developed LNP-based RNA therapies (siRNA or mRNA) for the respiratory tract. Such optimized LNP systems could offer an early treatment strategy for viral respiratory tract infections such as COVID-19.

Methods: We generated a small library of six LNP formulations with varying helper lipid compositions and characterized their hydrodynamic diameter, size distribution and cargo entrapment properties. Next, we screened these LNP formulations for particle uptake and evaluated their potential for transfecting mRNA encoding green fluorescence protein (GFP) or SARS-CoV2 nucleocapsid-GFP fusion reporter gene in a human airway epithelial cell line *in vitro*. Following LNP-siGFP delivery, GFP protein knockdown efficiency was assessed by flow cytometry to determine %GFP+ cells and median fluorescence intensity (MFI) for GFP. Finally, lead LNP candidates were validated in Friend leukemia virus B (FVB) male mice via intranasal delivery of an mRNA encoding luciferase, using *in vivo* bioluminescence imaging.

Results: Dynamic light scattering revealed that all LNP formulations contained particles with an average diameter of <100 nm and a polydispersity index of <0.2. Human airway epithelial cell lines in culture internalized LNPs with differential GFP transfection efficiencies (73–97%). The lead formulation LNP6 entrapping *GFP* or *Nuc-GFP* mRNA demonstrated the highest transfection efficiency (97%). Administration of LNP-*GFP* siRNA resulted in a significant reduction of GFP protein expression. For *in vivo* studies, intranasal delivery of LNPs containing helper lipids (DSPC, DOPC, ESM or DOPS) with *luciferase* mRNA showed significant increase in luminescence expression in nasal cavity and lungs by at least 10 times above baseline control.

Conclusion: LNP formulations enable the delivery of RNA payloads into human airway epithelial cells, and in the murine respiratory system; they can be delivered to nasal mucosa and lower respiratory tract via intranasal delivery. The composition of helper lipids in LNPs crucially modulates transfection efficiencies in airway epithelia, highlighting their importance in effective delivery of therapeutic products for airways diseases.

1. Introduction

To date, the novel coronavirus disease 2019 (COVID-19) pandemic has resulted in ~525 million infected individuals and caused 6.2+ million deaths across 191 countries (Anon, 2022). Although more than 11 billion COVID-19 vaccines have been administered globally, LNP-based COVID-19 mRNA vaccines from Pfizer/BioNTech, Moderna or other manufacturers present reduced protection against

* Corresponding author.
E-mail address: cjlim@mail.ubc.ca (C. Lim).

https://doi.org/10.1016/j.ejps.2022.106234
Received 10 January 2022; Received in revised form 6 June 2022; Accepted 7 June 2022
Available online 8 June 2022

asymptomatic (or mild) infections (Polack et al., 2020; Jackson et al., 2020; Andrews et al., 2022). Although the antibodies generated from the vaccines can be detected in circulation, it is unclear whether immune protection also occurs in the airway mucosa, the site of primary infection. Here, we propose the development of a general topical therapeutic solution for the nasal cavity, which involves the encapsulation of RNA using clinically-validated lipid nanoparticle (LNP) technology (Akinc et al., 2019) that can be used as a platform to prevent upper respiratory tract viral infections caused by pathogens such as the severe acute respiratory syndrome coronavirus 2 (SARS-CoV-2).

COVID-19 is caused by SARS-CoV-2, which uses its S-spike protein to bind the angiotensin converting enzyme (ACE) 2 on the surface of airway epithelial cells and gain entry into the host (Lan et al., 2020; Shang et al., 2020). Upon cellular entry, the viral RNA genome uses the host machinery to synthesize viral mRNA, proteins, and genomic RNA to produce replicate virions, which over time are released into the surrounding environment, enabling infection of adjacent cells. ACE2 is expressed on all epithelial cells in the respiratory tract, with the highest expression levels on cells lining the nasal cavity (Sungnak et al., 2020). This explains why SARS-CoV2 infection starts most commonly in the nasopharynx and progresses over several days to the lower airways (in approximately 10 to 20% of patients) where it causes pneumonia (Sungnak et al., 2020).

Nanomedicines are revolutionizing the treatment of diseases by enabling efficient delivery of nucleic acid materials to specific organs of interest. The key features of LNP include the four lipid components: (1) ionizable cationic lipid, (2) cholesterol, (3) structural helper lipid and (4) polyethylene glycol (PEG) lipid (Kulkarni et al., 2019a). LNP is essential for gene therapy as therapeutic delivery of free nucleic acid to target tissues is impaired by its inherent unfavorable physicochemical characteristics (*e.g.* negative charge of the nucleic acid backbone) as well as physiological barriers within the host (*e.g.* proteolytic attack by circulating serum nucleases). Efficiencies may be markedly improved by the use of LNPs. This has been demonstrated in the liver where the remarkable affinity of endogenous apolipoprotein E (ApoE) adsorbed to the LNP and its subsequent binding to the low density lipoprotein (LDL) receptors on hepatocytes allows for the internalization of the LNPs via endocytosis following intravenous administration (Akinc et al., 2019). Importantly, specific LNP delivery to the lungs has been demonstrated by nebulization (Zhang et al., 2020; Lokugamage et al., 2021); however, LNPs aerosolized using a nebulizer showed an increase in particle size and decreased encapsulation attributed to shear forces impacting the particle (Qiu et al., 2022). As well, intravenous LNP delivery to the lungs has been shown through optimization of the ionizable lipid (Adams et al., 2018); however, in such cases, custom synthesis of such molecules is typically necessary.

In general, upon acidification of the endosomal compartment, protonation of the ionizable lipid promotes LNPs' fusion with the anionic lipids of the endosomal membrane leading to subsequent membrane destabilization and release of their nucleic acid cargo into the cytoplasm. For example, LNPs have been used to deliver small interfering RNA (siRNA) into the cytoplasm of target cells, causing repression of the RNA machinery of the host cells (Andrews et al., 2022). This concept has been translated clinically in the approval of ONPATTRO ® (patisiran), the first siRNA-based LNP therapy that specifically inhibits hepatic synthesis of transthyretin (Adams et al., 2018). Here, we extend the utility of LNPs beyond the liver by developing LNPs that are capable of targeting airway epithelial cells via inhalational route that is non-invasive. We characterized LNP formulations containing different helper lipids—1,2-distearoyl-sn-glycero-3-phosphocholine (DSPC), 1,2-dioleoyl-sn-glycero-3-phosphocholine (DOPC), 1,2-dioleoyl-sn-glycero-3-phosphoethanolamine (DOPE), 1,2-dioleoyl-sn-glycero-3-phospho-(1′-rac-glycerol) (DOPG), egg sphingomyelin (ESM) and 1,2-dioleoyl-sn-glycero-3-phospho-L-serine (DOPS), which may play a major role in determining efficiency of uptake by host cells (Tam et al., 2021; Kulkarni et al., 2018; Kulkarni et al., 2019b).

2. Materials and methods

2.1. Preparation of lipid nanoparticles

Lipid nanoparticles (LNPs) were prepared by injecting volumes of lipid mixture (ionizable cationic lipid/structural lipid/cholesterol/PEG-DMG) at respective mol% ratios of 50/10/38.5/1.5 dissolved in ethanol to a final lipid concentration of 10 mM with an aqueous phase containing siRNA (amine-to-phosphate (N/P) ratio of 3) or mRNA (N/P ratio of 6) dissolved in 25 mM sodium acetate (pH 4) through a T-junction at a 3:1 aqueous:ethanol (v/v) ratio. Flow rates were set to 5 mL/min for the lipid phase and 15 mL/min for the aqueous phase culminating in an output flow rate of 20 mL/min. The resulting formulations were then dialyzed in Spectra/Por 2 12–14 kD MWCO dialysis tubing (Spectrum Labs) against 1000-fold volume of phosphate-buffered saline (pH 7.4) over a period of 24 h to remove ethanol from the formulation.

All lipids described in the study were commercially purchased from Avanti Polar Lipids. While the percentages of ionizable lipid, cholesterol and PEG-DMG remained constant, six different structural lipids (DSPC, DOPC, DOPE, DOPG, ESM and DOPS) were used. Lipid components dissolved in ethanol (10 mM total lipid) were combined with 25 mM sodium acetate pH 4 and dialyzed into the same buffer to remove solvent. The resulting pre-formed vesicles were concentrated and stored at 4 °C and used within two weeks. Using a benchtop-mixing procedure described elsewhere (Chen et al., 2016), we combined mRNA with LNP at a ratio of 29 μg RNA per μmol lipid immediately before dilution into cell media.

2.2. Analysis of lipid nanoparticles

Nucleic acid entrapment was measured using Quant-iT Ribogreen RNA (ThermoFisher) reagent following a standard procedure described elsewhere (Kulkarni et al., 2020). Particle size was quantified by dynamic light scattering performed on a Malvern Zetasizer NanoZS.

2.3. In-vitro transfections of GFP, NUC-GFP mRNA and GFP siRNA

The 1HAEo human airway epithelial cell line was obtained from Dr. Dieter Gruenert (UCSF) (Gruenert et al., 1988) and cultured in DMEM (Invitrogen) with 10% fetal bovine serum-FBS (ThermoFisher 12483020) and 1% penicillin-streptomycin (ThermoFisher 15140122) in a humidified 37 °C incubator with 5% CO_2. Cells were passaged at a confluence of greater than 70%. Briefly, cells were rinsed in phosphate-buffered saline (PBS), then detached with 0.25% trypsin + 0.53 mM EDTA at 37 °C. Trypsin was neutralized with addition of fresh media, the cells pelleted by centrifugation (1200 RPM for 8 min) and dispensed in a new plate using a subcultivation ratio of 1:3. Media was additionally changed every other day. First, to validate the transfection efficiency of the developed LNP system, CleanCap Green Fluorescence Protein (*GFP*) mRNA (L-7201; Trilink Biotech) was encapsulated and used for transfection of 1HAEo cells at a final concentration of 3 μg/mL for 24 h. Lipofectamine 3000 (heretoforth referred to as lipo3000) was used as a positive control for the transfection of *GFP* mRNA. Second, LNP-mRNA uptake efficiency was evaluated by incorporation of the non-exchangeable lipid dye DiD (1,1-dioctadecyl-3,3,3,3-tetramethylindodicarbocyanine) at 0.2 mol%.

For gene silencing, we used siRNA technology in different formulations of lipid nanoparticles or lipo3000 as positive controls (L3000015; ThermoFisher). For these experiments, cells were cultured in 10% FBS and pre-treated with 50 nM silencer-select scrambled or *GFP* siRNA (ThermoFisher 4390843 or s19753) for 24 h, followed by another round of siRNA treatment in the presence or absence of *GFP* mRNA (termed Tfn I) or a full length SARS-CoV2 structural gene (Nucleocapsid-Nuc) fused

Table 1
Physical properties of lipid nanoparticles for *in-vitro* screening.

LNP formulation	Surface charge	Helper lipids	Number-wt Particle Size (nm)	Size distribution (PDI)
1	neutral	DSPC	64.09	0.061
2	neutral	DOPC	68.95	0.114
3	neutral	DOPE	66.23	0.064
4	negative	DOPG	77.36	0.086
5	neutral	ESM	72.31	0.047
6	negative	DOPS	73.90	0.110

DSPC (1,2-Distearoyl-sn-glycero-3-phosphocholine).
DOPC (1,2-Dioleoyl-sn-glycero-3-phosphocholine).
DOPE (1,2-Dioleoyl-sn-glycero-3-phosphoethanolamine).
DOPG (1,2-di-(9Z-octadecenoyl)-sn-glycero-3-phospho-(1′-rac-glycerol)).
ESM (N-hexadecanoyl-D-erythro-sphingosylphosphorylcholine).
DOPS (1,2-di-(9Z-octadecenoyl)-sn-glycero-3-phospho-L-serine).
PDI – polydispersity index.

in-frame to *GFP* (*Nuc-GFP* mRNA) (termed Tfn II) as a reporter for 24 h, both of which were co-encapsulated in any given LNP formulation. LNP formulations were ranked in terms of *GFP* mRNA transfection efficiency for further *in-vitro* and *in-vivo* testing (Table 1).

To demonstrate whether *GFP* mRNA knockdown efficiency is dependent on the use of different helper lipids in an LNP system, 1HAEo cells were pre-treated with 50 nM silencer-select scrambled siRNA as an internal control or *GFP* siRNA using the top 2-ranked (DOPS or DOPC) and bottom 2-ranked (ESM or DSPC) helper lipids LNP system (Tfn I), followed by another round of siRNA treatment that was individually-encapsulated in DOPS, DOPC, ESM or DSPC (Tfn III) and in the presence or absence of *GFP* mRNA encapsulated in the top 2 (DOPS or DOPC) helper lipids in an LNP system.

2.4. Flow cytometry analysis

To assess the percentages of GFP+ and DiD+ cells post LNP-mRNA transfection, 1HAEo cells were analyzed by flow cytometry (Gallios, Beckman Coulter). Briefly, cells were lifted with trypsin (Invitrogen 25200056) for 2 min at 37 °C followed by neutralization with 10% FBS DMEM media and resuspended in phosphate-buffered solution (PBS) supplemented with 2% FBS. Kaluza for Gallios acquisition software (Beckman Coulter) was used to analyze the % GFP+ cells, mean fluorescence intensity (MFI) of % GFP+, % DiD+ cells and MFI of % DiD+ cells.

2.5. In-vivo transfection of LNPs

Male FVB/N (FVB) mice aged 8 weeks were obtained from an in-house founder colony using breeders from Jackson Laboratories (Bar Harbor, ME). To titrate a physiologically relevant dose of *luciferase* mRNA using luminescence reading as a surrogate of transfection, mice were anesthetized using isofluorane followed by administration of LNPs encapsulated with 0.25, 0.5 or 1.25 mg/kg CleanCap Firefly luciferase mRNA (5moU) (L7202 Trilink) injected intravenously into the mouse tail vein as positive controls for delivery in the livers (Kim et al., 2020). To evaluate the transfection ability of LNPs in the respiratory tract, mice were initially anesthetized with 2% isofluorane prior to an intranasal dispense of 50 μL LNP by pipette onto a single nostril with spontaneous inhalation (0.5 mg/kg). Experimental procedures were approved by the Animal Care Committee (Protocol # A15–0113) of the University of British Columbia based on guidelines provided by the Canadian Committee on Animal Care.

2.6. Bioluminescence imaging

Bioluminescence imaging was performed on an Ami-x (Spectral Instruments Imaging, Tucson, AZ, USA). Mice were anesthetized with 2% isoflurane followed by intranasal or intraperitoneal administration of D-luciferin (GoldBio, LUCK-1 G) and at a dose of 33 mg/kg @50 ul and 100 mg/kg @150 ul, respectively. While sedated on 2% isoflurane via a nose cone in the imaging platform, mice were imaged at 10 min post-administration of D-luciferin using an exposure time of 30 s at a bin of

Table 2
Ranking of lipid nanoparticles by %GFP transfection efficiency in 1HAEo cells.

LNP	% GFP	MFI GFP	% DiD	MFI DiD	rank
Empty lipid carrier	1.63	5242	–	–	–
Lipo3000-*GFP* mRNA	43.2	23,673	–	–	7
LNP1 (DSPC) – *GFP* mRNA	72.7	14,228	99.98	50,008	6
LNP2 (DOPC) – *GFP* mRNA	92.5	112,337	99.93	241,905	2
LNP3 (DOPE) – *GFP* mRNA	85.8	47,556	100	234,195	4
LNP4 (DOPG) – *GFP* mRNA	91.5	39,066	99.98	86,880	3
LNP5 (ESM) – *GFP* mRNA	84.9	20,580	99.97	114,048	5
LNP6 (DOPS) – *GFP* mRNA	96.5	260,930	99.98	235,359	1

GFP – green fluorescence protein.
MFI – median fluorescence intensity.
DiD – Lipophilic carbocyanine fluorescent dyes for membrane labeling.

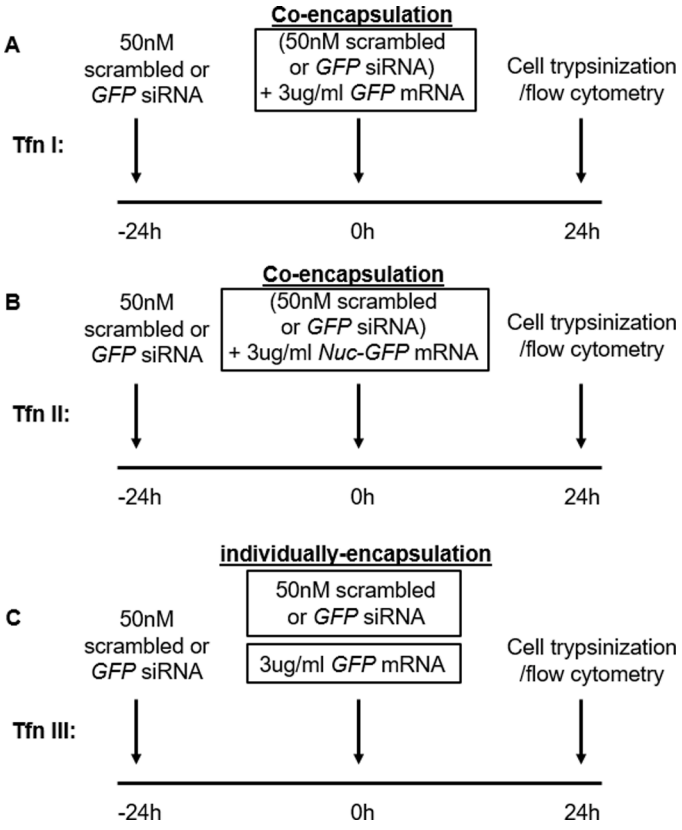

Fig. 1. *In vitro* transfection models according to timelines. (A) 1HAEo cells were pre-treated with 50 nM of scrambled or *GFP* siRNA for 24 h, followed by refreshment of a co-encapsulation treatment containing 50 nM of scrambled or *GFP* siRNA + 3 μg/mL *GFP* mRNA in lipo3000, LNP1 (DSPC), LNP2 (DOPC), LNP3 (DOPE), LNP4 (DOPG), LNP5 (ESM) or LNP6 (DOPS) (Tfn I). (B) 1HAEo cells were pre-treated with 50 nM of scrambled or *GFP* siRNA for 24 h, followed by refreshment of a co-encapsulation treatment containing 50 nM of scrambled or *Nuc-GFP* siRNA + 3 μg/mL *GFP* mRNA in lipo3000, LNP1 (DSPC), LNP2 (DOPC), LNP3 (DOPE), LNP4 (DOPG), LNP5 (ESM) or LNP6 (DOPS) (Tfn II). (C) 1HAEo cells were pre-treated with 50 nM of scrambled or *GFP* siRNA for 24 h, followed by refreshment of a individually-encapsulation treatment containing 50 nM of scrambled or *Nuc-GFP* siRNA + 3 μg/mL *GFP* mRNA in lipo3000, LNP1 (DSPC), LNP2 (DOPC), LNP3 (DOPE), LNP4 (DOPG), LNP5 (ESM) or LNP6 (DOPS) (Tfn III). All cells were trypsinized and subjected to flow cytometry 24 h post treatment.

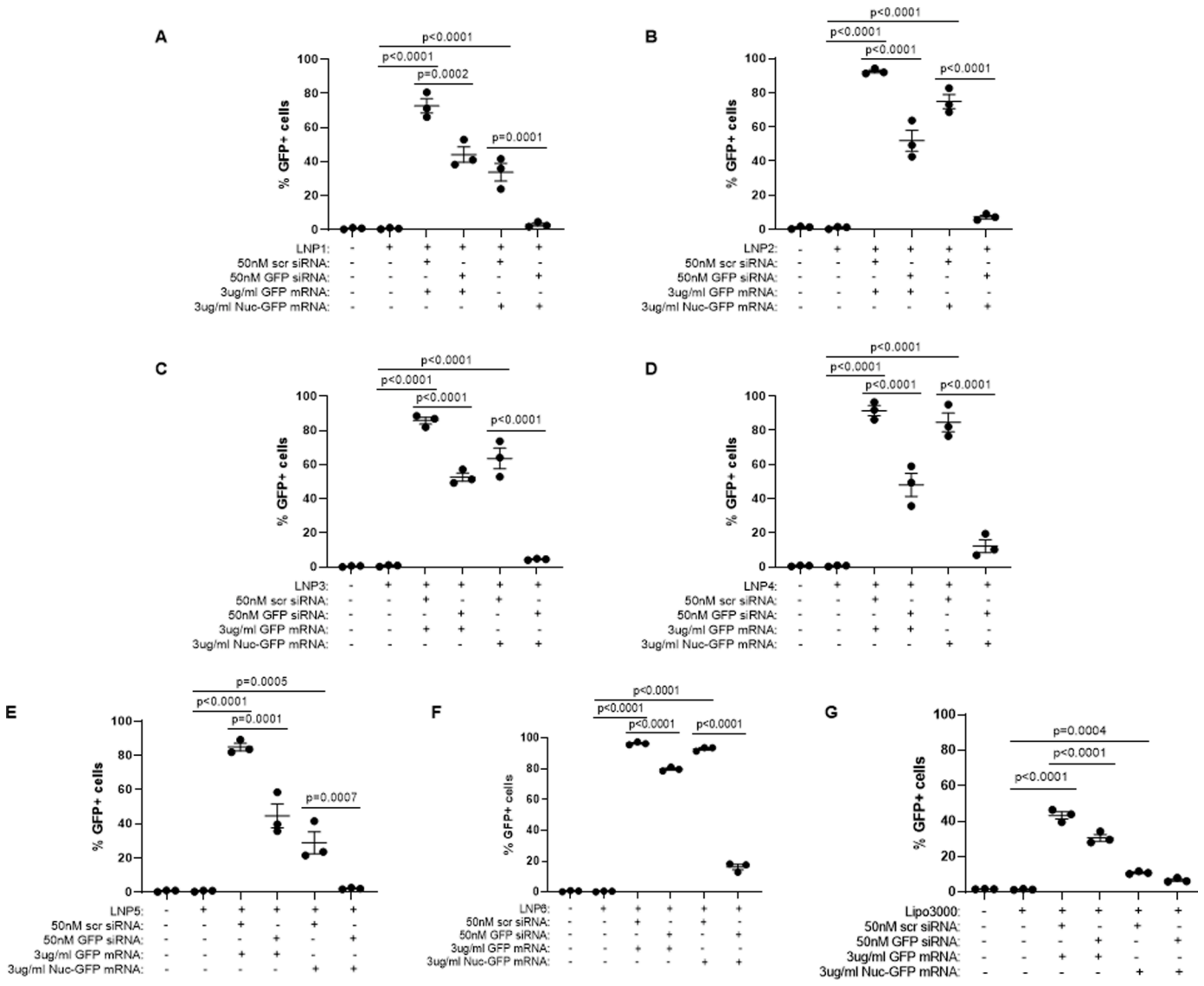

Fig. 2. Evaluating transfection by determining knockdown efficiency of *GFP* or *Nuc-GFP* mRNA using *GFP* siRNA expressed as % GFP+ in 1HAEo cells by flow cytometry. Quantification of % GFP+ 1HAEo cells pre-treated with 50 nM of scrambled or *GFP* siRNA for 24 h, followed by refreshment of (scrambled or *GFP* siRNA) + (3 μg/mL GFP mRNA via Tfn I or *Nuc-GFP* mRNA via Tfn II) co-encapsulated with, (A) LNP1 (DSPC), (B) LNP2 (DOPC), (C) LNP3 (DOPE), (D) LNP4 (DOPG), (E) LNP5 (ESM), (F) LNP6 (DOPS) and (G) lipo3000. Values were expressed as mean ± SEM ($N = 3$ independent experiments). One-way analysis of variance with Bonferroni's multiple comparisons test was used in panels A-G.

2 and ensuring that the acquired signal was within the detection range. Bioluminescence intensity was quantified by measuring the total emission flux (photons/ second) in the region of interest using the Spectral Imaging system software (AMI).

2.7. Statistical methods

Data were tested for normality prior to the selection of a parametric (normal distribution) or Mann Whitney (non-normal distribution) *t*-test, Kruskal Wallis multiple comparisons test, one-way ANOVA with Bonferroni's multiple comparisons test, and linear regression test, where appropriate. All data were analyzed using GraphPad Prism 8 (GraphPad Software Inc) and were expressed as mean ± SEM. Statistical significance was considered at $P < 0.05$.

3. Results

3.1. Characterization of lipid nanoparticles for in-vitro and in-vivo screening

The physical properties of LNP formulations #1–6 are summarized in Table 1. Our LNP formulations covered a range of structural lipids that could influence the surface charge and fluidity of the LNP membranes. The hydrodynamic size of the LNPs ranged from 64.09 to 77.36 nm with a polydispersity index (PDI) that ranged from 0.047 to 0.114. Using flow cytometry, we showed that *GFP* mRNA encapsulated in DOPS resulted in the highest transfection efficiency based on the proportion of GFP positive (GFP+) 1HAEo cells (96.5%). This was followed by DOPC (92.5%), DSPG (91.5%), DOPE (85.8%), ESM (84.9%), DSPC (72.7%) and lipo3000 (43.2%) compared to their respective empty lipid carrier controls (Table 2). Collectively, these data demonstrated that LNP encapsulation of *GFP* mRNA dramatically improved transfection efficiency compared to traditional methods involving lipofectamine. LNP particles composed of DOPS or DOPC as structural lipids exhibited the

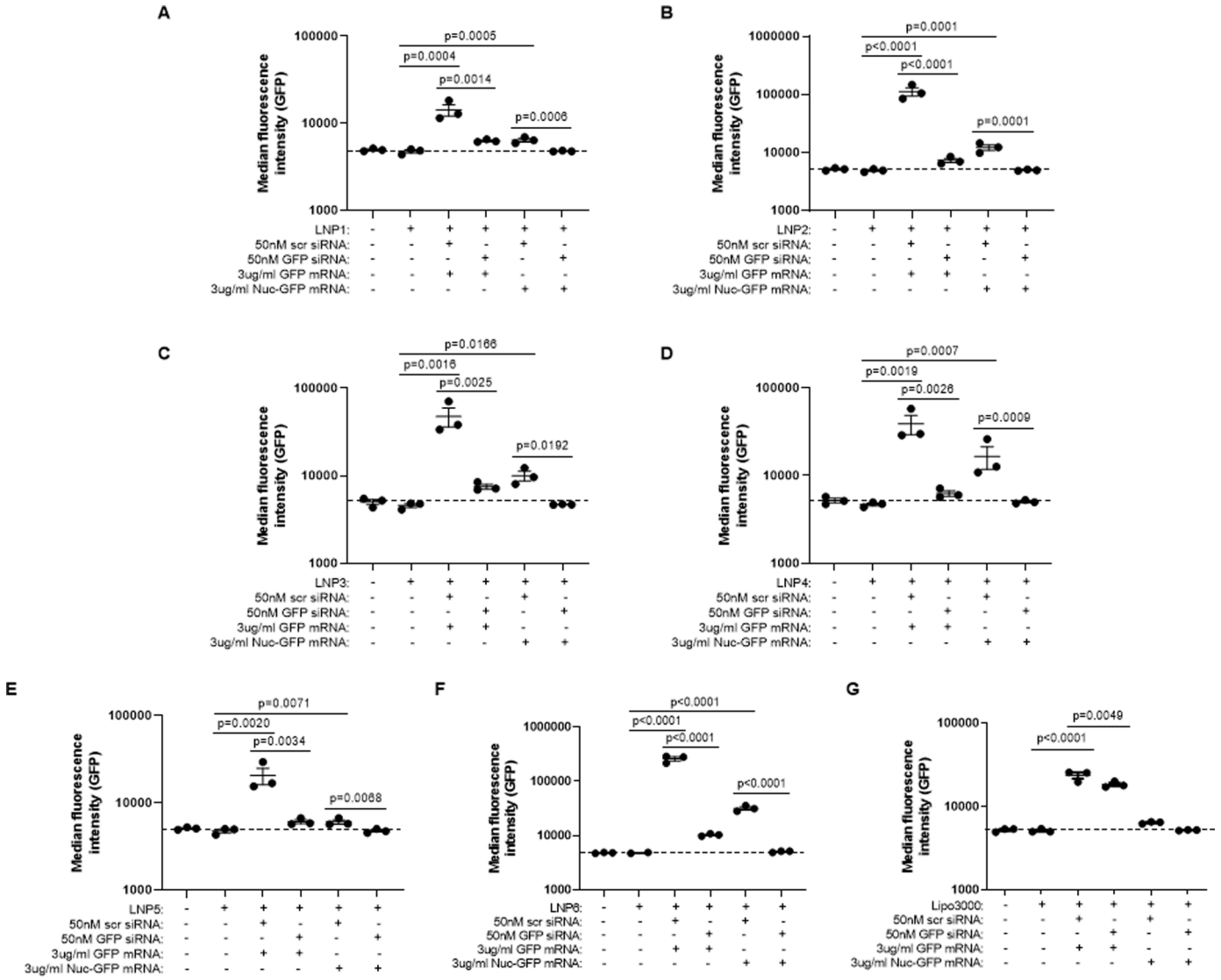

Fig. 3. Evaluating transfection by determining knockdown efficiency of *GFP* or *Nuc-GFP* mRNA using *GFP* siRNA expressed as MFI of GFP+ 1HAEo cells by flow cytometry. Quantification of median fluorescence intensity (MFI) of GFP+ 1HAEo cells pre-treated with 50 nM of scrambled or *GFP* siRNA for 24 h, followed by refreshment of (scrambled or *GFP* siRNA) + (3 μg/mL GFP mRNA via Tfn I or *Nuc-GFP* mRNA via Tfn II) when transfected simultaneously with (A) LNP1 (DSPC), (B) LNP2 (DOPC), (C) LNP3 (DOPE), (D) LNP4 (DOPG), (E) LNP5 (ESM), F) LNP6 (DOPS) and G) lipo3000. Values are expressed as mean ± SEM ($N = 3$ independent experiments). One-way analysis of variance with Bonferroni's multiple comparisons test was used in panels A-G.

greatest efficiency.

3.2. Co-encapsulation of siRNA/mRNA using DSPC and DOPS as helper lipids results in high transfection efficiency and uptake

Fig. 1A-C show the three different methods to evaluate the transfection (TfnI, TfnII, TfnIII) of *GFP* or *Nuc-GFP* mRNA in 1HAEo cells in our study. Transfection using all six LNP formulations and lipo3000 significantly increased the % GFP+ cells (Fig. 2A-G) and MFI of GFP (Fig. 3A-G) compared to their empty lipid carrier controls. Strikingly, all LNP-mediated transfections of *GFP* or *Nuc-GFP* mRNA were significantly higher than lipo3000-mediated transfections. GFP siRNA significantly reduced % GFP+ cells and MFI of GFP after LNP or lipo3000-mediated transfection of *GFP* or *Nuc-GFP* mRNA, respectively (Figs. 2A-G and 3A-G). DiD-co-labeling on all LNP-treated groups resulted in 100% DiD+ cells (Supplement Fig. 1), indicating LNP uptake in 100% of cells. All LNP formulations loaded with *GFP* or *Nuc-GFP* mRNA except for LNP4 had significantly higher lipid uptake (MFI of DiD) than empty lipid carrier (Supplement Fig. 2A-F). There was a strong consistency between transfection efficiency (% GFP+) and lipid uptake (MFI of DiD) for LNP2 (DOPC) and LNP6 (DOPS) (Table 2). Taken together, these results showed that the transfection efficiency and lipid uptake were dependent on helper lipid compositions in the LNPs.

3.3. Co-encapsulation of siRNA and mRNA has desirable knockdown efficiency

In Fig. 2, we show that co-encapsulation of *GFP* siRNA with *GFP* mRNA resulted in efficient knockdown of GFP protein expression across all LNP formulations (Fig. 2) and with DOPS demonstrating the greatest efficacy with an efficiency of 96.5% of cells positive for GFP (Table 2). To demonstrate whether individually encapsulating *GFP* mRNA and *GFP* siRNA affected the transfection efficiency, we chose the top 2 lipid carrier candidates (DOPC and DOPS) that showed superior transfection efficiencies, 92.5 and 96.5%, respectively (Table 2). Consistent with our co-encapsulation data, individually-encapsulated mRNA with DOPS resulted in superior transfection than that with DOPC as evaluated by % GFP and MFI of GFP. In contrast, treatment of *GFP* siRNA encapsulation

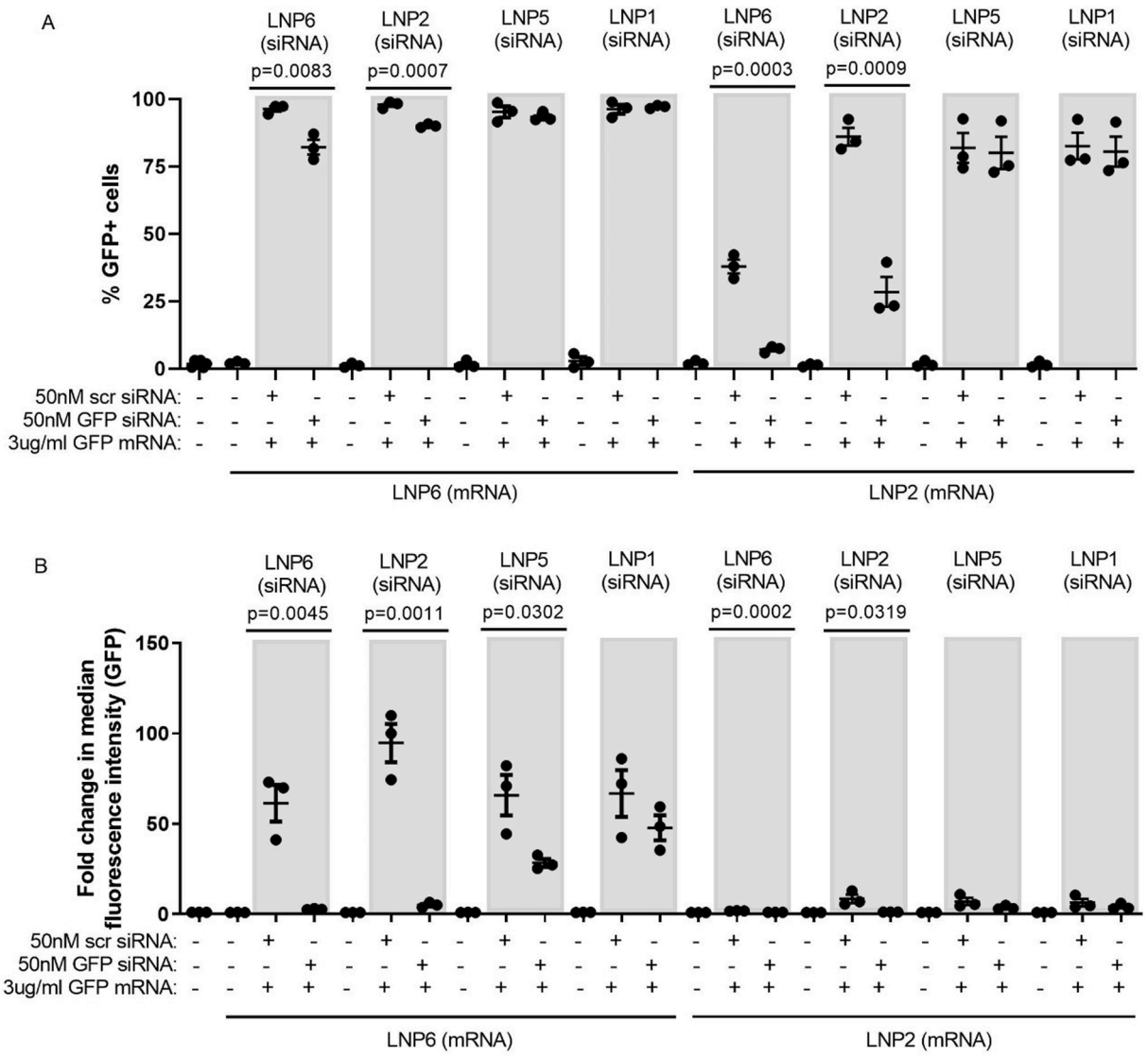

Fig. 4. Determining knockdown efficiency of *GFP* mRNA by individually-encapsulated *GFP* siRNA with different helper lipids. Quantification (A) % GFP+ and (B) median fluorescence intensity (MFI) of GFP+ 1HAEo cells pre-treated with 50 nM of scrambled or GFP siRNA encapsulated in LNP6 (DOPS), LNP2 (DOPC), LNP5 (ESM) or LNP1 (DSPC) for 24 h, followed by refreshment of (scrambled or *GFP* siRNA in each of the LNP) + 3 μg/mL *GFP* mRNA that were individually-encapsulated in LNP6 (DOPS) or LNP2 (DOPC) for another 24 h. Values were expressed as mean ± SEM ($N = 3$ independent experiments). One-way analysis of variance with Bonferroni's multiple comparisons test was used in panels A-B.

with the bottom 2 lipid carrier candidates (ESM and DSPC) failed to achieve the desired knockdown efficiency (Fig. 4A). All LNP uptake into cells were shown to have 100% DiD+ cells as indicated by DiD-co-labeling (Supplement Fig. 3A). Interestingly, we showed that empty LNPs without mRNA or siRNA had significantly increased MFI of DiD compared to untreated control but had approximately 50% lower MFI of DiD compared with LNPs loaded with mRNA or siRNA (Supplement Fig. 3B). Collectively, we showed that mRNA and siRNA can be co-encapsulated in the same LNP to deliver potent transfection and increase uptake potentials.

3.4. Evaluation of knockdown efficiency for individually encapsulated or co-encapsulated siRNA and mRNA

In Fig. 2, we demonstrated that co-encapsulation of *GFP* siRNA with *GFP* mRNA resulted in efficient knockdown of GFP protein expression across all LNP formulations. Next, we evaluated the transfection efficiency using a modified protocol, where *GFP* mRNA and *GFP* siRNA were individually encapsulated (Tfn III in Fig. 1C) using the top 2 lipid carrier candidates (DOPC and DOPS) with the highest transfection efficiencies (Table 2). *GFP* mRNA encapsulated in DOPS (LNP6) achieved the highest transfection efficiencies in terms of % GFP+ (Fig. 4A) and MFI GFP (Fig. 4B) when compared to DOPC (LNP2), regardless of the LNP formulation used to encapsulate siRNA. However, use of DOPS (LNP6) to encapsulate scrambled siRNA reduced the transfection rate of DOPC (LNP2) encapsulated *GFP* mRNA (Fig. 4A). In contrast, the combination of DOPC (LNP2) encapsulated siRNA with DOPS (LNP6) encapsulated *GFP* mRNA resulted in the highest GFP expression level as well as knockdown efficiency (Fig. 4B). We also noted that *GFP* siRNA encapsulated in the bottom 2 lipid carrier candidates (ESM and DSPC) failed to achieve the desired knockdown efficiency (Fig. 4A). When comparing the results between co-encapsulated and individually encapsulated methods, we conclude that co-encapsulation of mRNA and siRNA with the same LNP is an efficient transfection method to achieve high expression of mRNA coupled with efficient knockdown with the targeted siRNA.

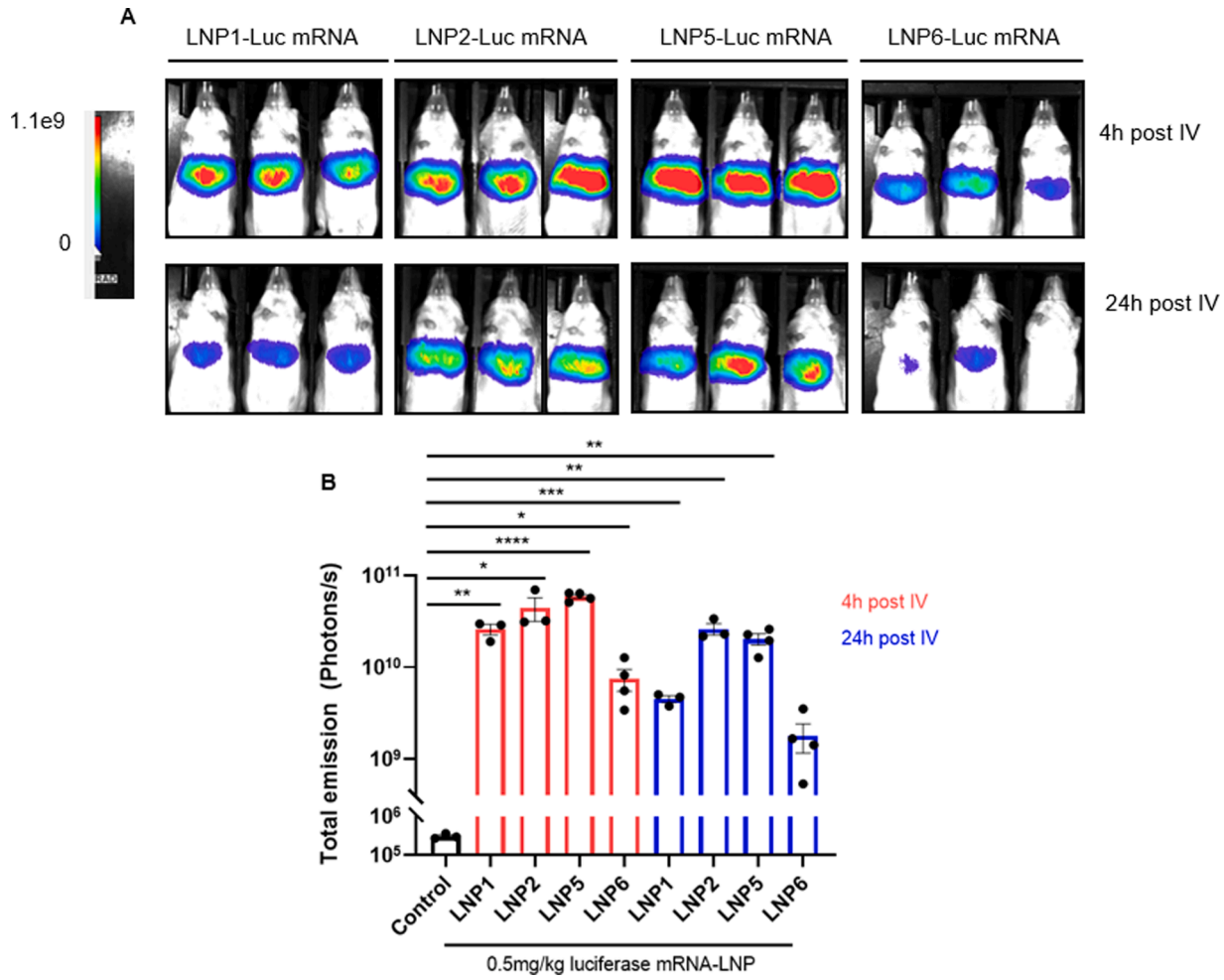

Fig. 5. Intravenous (IV) delivery of LNP-luciferase mRNA as positive control of liver transfection *in-vivo*. (A) FVB mice receiving an IV delivery of 0.5 mg/kg luciferase mRNA encapsulated in LNP1 (DSPC), LNP2 (DOPC), LNP5 (ESM) or LNP6 (DOPS) were imaged and (B) quantified using IVIS at 4 h or 24 h post LNP treatment. Values were expressed as mean ± SEM ($N = 3$–4). One-way analysis of variance with Bonferroni's multiple comparisons test was used in panel B. Control untreated mice were not shown but also received intranasal delivery of luciferin for signal acquisition.

3.5. Optimal in-vivo LNP transfection and expression of luciferase mRNA are tissue dependent

As a positive control of liver hepatocyte transfection *in-vivo*, LNP packaged *luciferase* mRNA was administered intravenously (IV) into mice via tail vein injection. LNP formulations composed of DSPC, DOPC, ESM and DOPS as structural lipids exhibited greater transfection efficiency at 4 h than at 24 h post-injection as represented by luciferase-mediated bioluminescence emission (Figs. 5A, B, Supplement Fig. 4). Liver transfection using DOPS (LNP6) consistently showed lower expression amongst other formulations at both 4 and 24 h time points (Figs. 5A, B, Supplement Fig. 4).

Lastly, we evaluated the ability for LNP packaged *luciferase* mRNA to transfect airway epithelial cells when delivered intranasally. LNP formulations composed of DSPC, DOPC, ESM, or DOPS successfully transfected mucosal cells within the nasal cavity and lungs at 4 h post-intranasal administration and remained detectable at 24 h (Fig. 6). Interestingly, luciferase signals measured in the nasal cavity was highest at 4 h following intranasal delivery with DOPS as a structural lipid, while signals resulting from DSPC, DOPC, and ESM lipids increased between 4 h and 24 h (Fig. 6B). In contrast, measurement of signals originating from lungs indicated luciferase activity was higher for all four lipids at 4 h when compared to 24 h, and that DOPC and ESM conferred the highest transfection rate in lungs.

4. Discussion

In this study, we demonstrated the feasibility of using LNP packaged RNA for intranasal administration of potential therapeutics targeting the airway epithelium. Specifically, we showed that high transfection efficiency can be achieved by local delivery of LNP-mRNA. In addition, transfection efficiencies can be enhanced by modulating helper lipids, indicating the potential for optimization and improvement of transfection efficiency. The optimization of these helper lipid compositions could lead to advances in the treatment of respiratory tract infections such as COVID-19 and chronic airway conditions such as asthma and cystic fibrosis (CF).

An *in vitro* LNP formulation screen using an airway epithelia cell line established helper lipids DOPS and DOPC as leading candidates with high transfection efficiency of target mRNA. Importantly, all screened LNP compositions achieved higher transfection efficiency of *GFP* mRNA compared to classical commercial liposomal formulations such as lipofectamine, indicating the benefits of LNP-mediated delivery. Further assessment of *in vitro* transfection and knockdown established the feasibility of LNP-mediated delivery of both mRNA and siRNA cargo. Importantly, co-encapsulation of *GFP* siRNA and mRNA achieved sufficient knockdown activity, obviating the need for separate encapsulation of siRNA and mRNA. This indicates the feasibility of designing a system that efficiently delivers both mRNA and siRNA simultaneously (if needed) to treat certain genetic defects associated with known diseases.

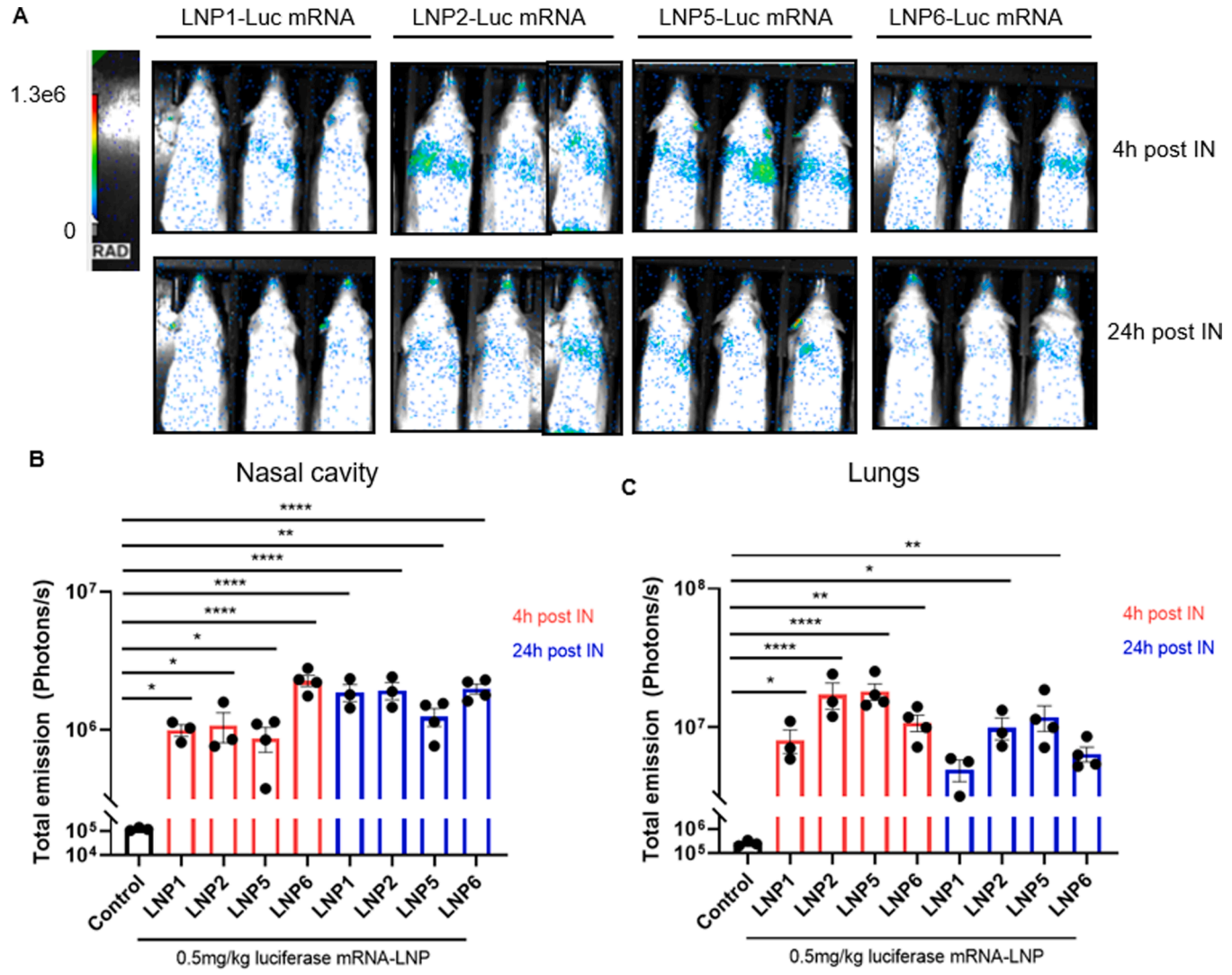

Fig. 6. Intranasal (IN) delivery of LNP-luciferase mRNA to evaluate transfection efficiency of different helper lipids *in-vivo*. (A) FVB mice receiving an IN delivery of 0.5 mg/kg luciferase mRNA encapsulated in LNP1 (DSPC), LNP2 (DOPC), LNP5 (ESM) or LNP6 (DOPS) were imaged and quantified using IVIS at 4 h or 24 h post LNP treatment in the (B) nasal cavity and (C) lung compartment. Values were expressed as mean ± SEM (N = 3–4). One-way analysis of variance with Bonferroni's multiple comparisons test was used in panels B and C. Control untreated mice were not shown but also received intranasal delivery of luciferin for signal acquisition.

The co-delivery of trastuzumab mRNA to produce anti-HER2 antibodies and siRNA targeting HER2 in HER2+ breast cancer is a contemporary example of the potential therapeutic potential for this approach (Shu et al., 2020). To maximize the use of both mRNA and siRNA in a single LNP-based therapy with added tissue specificity, we believe that it is important to optimize helper lipids and helper lipid concentrations. In the context of respiratory diseases, the most common cause of cystic fibrosis (CF) is due to the deletion of the phenylalanine amino acid at position 508 (F508del) in the CF transmembrane conductance regulator (*CFTR*) gene (Lukacs and Verkman, 2012). Previous studies have shown even partial rescue of the F508del mutation through siRNA or miRNA mediated knockdown of proteins that interact with CFTR leads to a significant improvement in the phenotype and thus is a viable therapeutic approach (Hutt et al., 2018a, 2018b; Tomati et al., 2015). However, the therapeutic potential for co-delivery of respective siRNA/miRNA and functional *CFTR* mRNA in CF requires further exploration.

A subsequent LNP formulation screen revealed a discordance between the *in vitro* and *in vivo* results. Specifically, the DOPS formulation appeared to be most efficacious in the nasal cavity after IN administration consistent with the *in vitro* data. On the other hand, ESM appeared to be one of the helper lipids that was most efficacious in lungs despite being a poor performer *in vitro*. It should be noted, however, that cell culture systems are representative of an ideal environment where LNPs can be delivered to target cells through ApoE in the presence of fetal bovine serum (FBS). The presence of LDL receptors expressed on human airway epithelial cells allows for the latter's use as an appropriate *in vitro* model for our experiments (Saraya et al., 2014). However, *in vivo* systems introduce a multitude of variables that may impede successful transfection. Many of these complications lie in the realm of pharmacokinetic and pharmacodynamic barriers in ligand-receptor interactions on the target tissues. For example, lower expression of required receptors in target tissues *in vivo* can dramatically reduce transfection levels due to diminished uptake. Interestingly, successful transfection was observed for LNPs administered via the nasal cavity, suggesting that ApoE-mediated uptake may not be the only route of internalization. A proposed mechanism relies on the relationship between particle size and location of particle deposition. Due to the size of the individual LNP particles, most of the particles deposit into the lungs by Brownian motion. Thus, LNP deposition in the lungs is likely mostly due to random chance (Thorley et al., 2014). The depth of deposition is also dependent on particle size, in which particles above 5 μm are

primarily filtered out in the upper airways and trachea (Darquenne, 2012). Only particles smaller than this diameter threshold can make it to the distal airways and alveoli. In a previous study, it has been shown that small nanoparticles can be taken up by human alveolar type I epithelial cells either through passive diffusion across plasma membranes or clathrin- or caveolae-mediated endocytosis (Thorley et al., 2014). This property allows for the subsequent expression of luciferase and its detection by IVIS in the lungs (Cheng et al., 2020).

Modulation of specific helper lipid present in the formulation can alter the transfection efficiency, suggesting that helper lipids are crucial in determining payload release into cells and therapeutic potential of LNP-based compounds. Indeed, it was shown in a previous study that the presence of internalized helper lipid is what allows for the stable encapsulation of nucleic acid (Kulkarni et al., 2019b), which is a consistent explanation for the fluctuation in transfection efficiency seen in the aforementioned experiments. Recent studies have also demonstrated that the LNP surface is composed of PEG lipid, structural helper lipid, and cholesterol while the LNP core consists of ionizable lipid and nucleic acid cargo (Cullis and Hope, 2017). As helper lipids are known to mediate destabilization of the endosomal membrane, it is plausible that any modulation in the structural helper lipid used during formulation may affect intracellular delivery and the transfection efficiency. Thus, we propose that these helper lipids produce their effects as a result of their tendency towards endosomal escape. In an *in vitro* setting, where LNPs are incubated with cells and allowed to be freely taken up, it is plausible that individual particle stability in complex medium is not as important as a factor, and their tendency to release their cargo upon endocytosis is likely the driving force behind the observed differences in transfection efficiency. For instance, the monounsaturated oleyl-derived helper lipids demonstrate higher transfection efficiency as compared to their saturated stearoyl-derived counterparts (Table 2). The unsaturation likely increases fluidity within the bilayers of the LNP in comparison to the rigidity of the stearoyl counterpart. The additional unsaturation component also increases the likelihood of endosomal release. Indeed, a previous study observed superior lipid fusion with lipids with unsaturated tails in comparison to their saturated counterparts (Lee et al., 2020). However, the *in vivo* setting presents different pharmacokinetic barriers that include absorption and prolonged exposure to a complex medium. Thus, particle stability plays an additional important role. This rationale helps to explain the contradictory transfection profile of ESM, where ESM was a helper lipid with decreased transfection efficiency in the *in vitro* screen, but the top helper lipid demonstrating transfection in the lungs alongside DOPC. Specifically, lipid polymorphism rationalizes that lipids have an overall cylindrical shape when the cross-sectional area of the headgroup is similar to the cross-sectional area of the acyl chains. In the case of phosphocholine (PC) lipids like DOPC and ESM, this leads to stable bilayer structures and more stable particles (van den Brink-van der Laan et al., 2004). DOPS on the other hand, has been characterized to undergo transitions to less stable non-bilayer phases (Fuller et al., 2003). Taken together, the decreased transfection profile shown by DOPS and performance of DOPC and ESM could be attributed to the additional factor of particle stability.

In the present study, we used an *in vitro* and *in vivo* LNP screen to demonstrate the feasibility of delivering RNA payloads to human airway epithelial cells. Limitations not addressed by this model include the inability of IVIS to determine the exact cell types where transfection occurred. However, a previous study reported that of all the LNP-transfected cells, 39% were epithelial cells, 66% were endothelial cells and 21% were immune cells (Cheng et al., 2020). Additionally, the LNP formulations utilized for these studies were not nebulized, which may have increased the variability of lung deposition across the animals.

5. Conclusion

In summary, this study demonstrates that high transfection efficiency can be achieved through LNP-mediated delivery of RNA payloads. Specifically, we showed the potential for co-delivery of siRNA and mRNA, which advances the potential for gene therapy in airways diseases. Additionally, we show that helper lipids are crucial for modulating LNP efficiency, highlighting their importance in LNP formulation for achieving maximal efficacy. This work provides insight into the mechanisms of LNP delivery in the airways, as well as the potential for new therapeutic or vaccine development for the treatment of genetic diseases.

CRediT authorship contribution statement

A Tam: Conceptualization, Methodology, Software, Validation, Formal analysis, Writing – original draft, Writing – review & editing, Project administration, Funding acquisition. **J Kulkarni:** Methodology, Software, Investigation, Resources. **K An:** Data curation, Visualization, Writing – review & editing. **L Li:** Project administration, Writing – review & editing. **DR Dorscheid:** Resources, Writing – review & editing. **GK Singhera:** Resources, Writing – review & editing. **P Bernatchez:** Resources, Writing – review & editing, Funding acquisition. **GSD Reid:** Resources, Writing – review & editing. **KYT Chan:** Resources, Writing – review & editing. **D Witzigmann:** Methodology, Resources. **PR Cullis:** Conceptualization, Resources. **DD Sin:** Conceptualization, Resources, Writing – review & editing, Supervision, Funding acquisition. **CJ Lim:** Conceptualization, Resources, Writing – review & editing, Visualization, Supervision, Funding acquisition.

Acknowledgments

AT is a recipient of a MITACS Accelerate fellowship award. PRC acknowledges support from the Canadian Institutes for Health Research (CIHR FDN 148469) and the NanoMedicines Innovation Network (NMIN), a Canadian Networks of Centres of Excellence (NCE) in nanomedicine. DW is supported by the Swiss National Science Foundation (#183923). JAK is supported by the NMIN Postdoctoral Fellowship Award in Gene Therapy. This study receives support from the Canadian Institute of Health Research (CIHR) and the BC Lung Association.

Supplementary materials

Supplementary material associated with this article can be found, in the online version, at doi:10.1016/j.ejps.2022.106234.

References

Anon, 2022 https://gisanddata.maps.arcgis.com/apps/opsdashboard/index.html#/bda7594740fd40299423467b48e9ecf6.

Polack, F.P., Thomas, S.J., Kitchin, N., Absalon, J., Gurtman, A., Lockhart, S., et al., 2020. Safety and efficacy of the BNT162b2 mRNA COVID-19 Vaccine. N. Engl. J. Med.

Jackson, L.A., Anderson, E.J., Rouphael, N.G., Roberts, P.C., Makhene, M., Coler, R.N., et al., 2020. An mRNA vaccine against SARS-CoV-2 - preliminary report. N. Engl. J. Med. 383 (20), 1920–1931.

Andrews, N., Stowe, J., Kirseborn, F., Toffa, S., Rickeard, T., Gallagher, E., et al., 2022. COVID-19 vaccine effectiveness aginst the Omicron (B.1.1.529) variant. N. Engl. J. Med. 386, 1532–1546.

Akinc, A., Maier, M.A., Manoharan, M., Fitzgerald, K., Jayaraman, M., Barros, S., et al., 2019. The Onpattro story and the clinical translation of nanomedicines containing nucleic acid-based drugs. Nat. Nanotechnol. 14 (12), 1084–1087.

Lan, J., Ge, J., Yu, J., Shan, S., Zhou, H., Fan, S., et al., 2020. Structure of the SARS-CoV-2 spike receptor-binding domain bound to the ACE2 receptor. Nature 581 (7807), 215–220.

Shang, J., Ye, G., Shi, K., Wan, Y., Luo, C., Aihara, H., et al., 2020. Structural basis of receptor recognition by SARS-CoV-2. Nature 581 (7807), 221–224.

Sungnak, W., Huang, N., Becavin, C., Berg, M., Queen, R., Litvinukova, M., et al., 2020. SARS-CoV-2 entry factors are highly expressed in nasal epithelial cells together with innate immune genes. Nat. Med.

Kulkarni, J.A., Witzigmann, D., Chen, S., Cullis, P.R., van der Meel, R., 2019a. Lipid nanoparticle technology for clinical translation of siRNA therapeutics. Acc. Chem. Res. 52 (9), 2435–2444.

Zhang, H., Leal, J., Soto, M.R., Smyth, H.D.C., Ghosh, D., 2020. Aerosolizable lipid nanoparticles for pulmonary delivery of mRNA through design of experiments. Pharmaceutics 12 (11), 1042.

Lokugamage, M.P., Vanover, D., Beyersdorf, J., Hatit, M.Z.C., Rotolo, L., Schrader, E., et al., 2021. Optimization of lipid nanoparticles for the delivery of nebulized therapeutic mRNA to the lungs. Nat. Biomed Eng. 5, 1059–1068.
Qiu, M., Tang, Y., Chen, J., Muriph, R., Ye, Z., Huang, C., et al., 2022. Lung-selective mRNA delivery of synthetic lipid nanoparticles for the treatment of pulmonary lymphangioleiomyomatosis. Proc. Natl. Acad. Sci. U. S. A. 119 (8).
Adams, D., Gonzalez-Duarte, A., O'Riordan, W.D., Yang, C.C., Ueda, M., Kristen, A.V., et al., 2018. Patisiran, an RNAi therapeutic, for hereditary transthyretin amyloidosis. N. Engl. J. Med. 379 (1), 11–21.
Tam, A., Leclair, P., Li, L.V., Yang, C.X., Li, X., Witzigmann, D., et al., 2021. FAM13A as potential therapeutic target in modulating TGF-beta-induced airway tissue remodeling in COPD. Am. J. Physiol. Lung Cell. Mol. Physiol.
Kulkarni, J.A., Darjuan, M.M., Mercer, J.E., Chen, S., van der Meel, R., Thewalt, J.L., et al., 2018. On the formation and morphology of lipid nanoparticles containing ionizable cationic lipids and siRNA. ACS Nano 12 (5), 4787–4795.
Kulkarni, J.A., Witzigmann, D., Leung, J., Tam, Y.Y.C., Cullis, P.R., 2019b. On the role of helper lipids in lipid nanoparticle formulations of siRNA. Nanoscale 11 (45), 21733–21739.
Chen, S., Tam, Y.Y.C., Lin, P.J.C., Sung, M.M.H., Tam, Y.K., Cullis, P.R., 2016. Influence of particle size on the *in vivo* potency of lipid nanoparticle formulations of siRNA. J. Control Rel. 235, 236–244.
Kulkarni, J.A., Thomson, S.B., Zaifman, J., Leung, J., Wagner, P.K., Hill, A., et al., 2020. Spontaneous, solvent-free entrapment of siRNA within lipid nanoparticles. Nanoscale 12, 23959–23966.
Gruenert, D.C., Basbaum, C.B., Welsh, M.J., Li, M., Finkbeiner, W.E., Nadel, J.A., 1988. Characterization of human tracheal epithelial cells transformed by an origin-defective simian virus 40. Proc. Natl. Acad. Sci. U. S. A. 85 (16), 5951–5955.
Kim, J., Jozic, A., Sahay, G., 2020. Naturally derived membrane lipids impact nanoparticle-based messenger RNA delivery. Cell. Mol. Bioeng. 1–12.
Shu, M., Gao, F., Yu, C., Zeng, M., He, G., Wu, Y., et al., 2020. Dual-targeted therapy in HER2-positive breast cancer cells with the combination of carbon dots/HER3 siRNA and trastuzumab. Nanotechnology 31 (33), 335102.
Lukacs, G.L., Verkman, A.S., 2012. CFTR: folding, misfolding and correcting the ΔF508 conformational defect. Trends Mol. Med. 18 (2), 81–91.
Hutt, D.M., Mishra, S.K., Roth, D.M., Larsen, M.B., Angles, F., Frizzell, R.A., et al., 2018a. Silencing of the Hsp70-specific nucleotide-exchange factor BAG3 corrects the F508del-CFTR variant by restoring autophagy. J. Biol. Chem. 293 (35), 13682–13695.
Hutt, D.M., Loguercio, S., Roth, D.M., Su, A.I., Balch, W.E., 2018b. Correcting the F508del-CFTR variant by modulating eukaryotic translation initiation factor 3-mediated translation initiation. J. Biol. Chem. 293 (35), 13477–13495.
Tomati, V., Sondo, E., Armirotti, A., Caci, E., Pesce, E., Marini, M., et al., 2015. Genetic Inhibition of the Ubiquitin Ligase Rnf5 Attenuates Phenotypes Associated to F508del Cystic Fibrosis Mutation. Sci. Rep. 5, 12138.
Saraya, T., Kurai, D., Ishii, H., Ito, A., Sasaki, Y., Niwa, S., et al., 2014. Epidemiology of virus-induced asthma exacerbations: with special reference to the role of human rhinovirus. Front. Microbiol. 5, 226.
Thorley, A.J., Ruenraroengsak, P., Potter, T.E., Tetley, T.D., 2014. Critical determinants of uptake and translocation of nanoparticles by the human pulmonary alveolar epithelium. ACS Nano 8 (11), 11778–11789.
Darquenne, C., 2012. Aerosol deposition in health and disease. J. Aerosol Med. Pulm. Drug Deliv. 25 (3), 140–147.
Cheng, Q., Wei, T., Farbiak, L., Johnson, L.T., Dilliard, S.A., Siegwart, D.J., 2020. Selective organ targeting (SORT) nanoparticles for tissue-specific mRNA delivery and CRISPR-Cas gene editing. Nat. Nanotechnol. 15 (4), 313–320.
Cullis, P.R., Hope, M.J., 2017. Lipid nanoparticle systems for enabling gene therapies. Mol. Ther. 25 (7), 1467–1475.
Lee, S.M., Cheng, Q., Yu, X., Liu, S., Johnson, L.T., Siegwart, D.J., 2020. A systematic study of unsaturation in lipid nanoparticles leads to improved mRNA transfection *in vivo*. Angew. Chem. Int. Ed. 60 (11), 5848–5853.
van den Brink-van der Laan, E., Killian, J.A., de Kruijff, B., 2004. Nonbilayer lipids affect peripheral and integral membrane proteins via changes in the lateral pressure profile. Biochim. Biophys. Acta Biomembr. 1666 (1–2), 275–288.
Fuller, N., Benatti, C.R., Rand, R.P., 2003. Curvature and bending constants for phosphatidylserine-containing membranes. Biophys. J. 85 (3), 1667–1674.